Visualization of Spatiotemporal Behavior of Discrete Maps via Generation of Recursive Median Elements

B.S. Daya Sagar, *Senior Member*, *IEEE*

Abstract—Spatial interpolation is one of the demanding techniques in Geographic Information Science (GISci) to generate interpolated maps in a continuous manner by using two discrete spatial and/or temporal data sets. Noise-free data (thematic layers) depicting a specific theme at varied spatial or temporal resolutions consist of connected components either in aggregated or in disaggregated forms. This short paper provides a simple framework: 1) to categorize the connected components of layered sets of two different time instants through their spatial relationships and the Hausdorff distances between the companion-connected components and 2) to generate sequential maps (interpolations) between the discrete thematic maps. Development of the median set, using Hausdorff erosion and dilation distances to interpolate between temporal frames, is demonstrated on lake geometries mapped at two different times and also on the bubonic plague epidemic spread data available for 11 consecutive years. We documented the significantly fair quality of the median sets generated for epidemic data between alternative years by visually comparing the interpolated maps with actual maps. They can be used to visualize (animate) the spatiotemporal behavior of a specific theme in a continuous sequence.

Index Terms—GISci, spatial interpolation, mathematical morphology, thematic maps, dilation, erosion, interpolation formulas, spatial databases and GIS, cartography, morphological image representation, visualization techniques and methodologies, geometrical problems and computations, set theory.

1 Introduction

SPATIAL interpolation techniques are used to develop an information system that is both scale and time-independent. The concepts from Geographic Information Science (GISci) provided new insights to develop information systems in spatial form further facilitating to visualize the relations between "layered information" (see, e.g., [1]). These thematic layers will be prepared—by computer-assisted mapping or by digitizing manually mapped information—from various sources of data acquired by remote sensing, field surveys, demographic surveys, historical records, etc. The important problem posed to the GIS community is the integration of temporal data available as snapshots of the ever-changing phenomena at discrete intervals [2], [3]. By using such snapshots as input layers depicting thematic information, the way of mapping algebraic concepts [4] extended with category theory [5] in order to generate an output layer is explained in [6]. Although [6] is not concerned with the focus of this paper on spatial interpolations, it is important for the reader to understand the data representation in layered format and the simple operations—such as addition, subtraction, and product—involved in generation of output layers from the temporal data.

In GISci, development of a theme-specific information system requires spatially represented thematic maps. Such maps, derived from data acquired either physically or remotely sensed, are usually stored in layered forms. Each layer represents in noise-free binary form a theme (foreground) and a no-theme (background). The layered information is available at different spatiotemporal scales. A usual limitation is that this information is not available in a continuous form, i.e., at all spatiotemporal resolutions. Deriving layers in continuous form from a limited set of layers (available at discrete intervals) requires a procedure discussed in this short note.

Predicting a spatial structure between two other spatial structures—which may be represented at two different spatial and/or temporal resolutions—evidently requires an interpolation procedure. "Spatial structure" and "spreading of a phenomenon" are interchangeably used here, though the phenomenon may evolve with time. In order to predict and visualize the spatiotemporal dynamics of a phenomenon between two time periods, one needs to generate (interpolate) the intermediary sequence of phenomena between the known time periods.

In the case of spatial maps, the available interpolation techniques include kriging [7], shape-based interpolation [8], [9], and Hausdorff-distance-based interpolation [10], [11], [12], [13], [14], [15], [16]. Other interpolation methods, to name a few, for binary objects include elastic dynamic interpolation [17], [18] and directional interpolation [19]. These algorithms [17], [18], [19] are computationally and algorithmically expensive and have limitations when dealing with nonconvex objects. While kriging yields promising results [6], this interpolation technique, in the context of geoscience and/or GISci, has only been used for spatial sets (layers). Moreover, kriging techniques are meant for global transforms that ignore the connectivity of components involved in the two input sets. To make use of a spatial interpolation technique in the context of GISci, particularly for spatiotemporal visualization, one needs to categorize the connected components (subsets), based on the spatial relationship between the companion-connected components that belong to two input sets of different spatial and/or temporal scales. The material that follows deals with: 1) categorization of the connected components by means of Hausdorff erosion and dilation distances and 2) use of the category-specific median-set computation recursively.

The paper is organized as follows: Basic morphological transformations, Hausdorff distance, and median set computation between two sets as a global transformation are explained in Section 2. In Section 3, spatially represented themes with different categories are identified with reference to logical relationships and Hausdorff distances. In Section 4, the application of morphologic interpolation to generate sequential interpolated layered information is explained. In the same section, experimental results will be presented for two cases: small water bodies at two different time periods and bubonic plague data. Sections 5 and 6 contain a brief discussion of the potential applications of the proposed framework in the context of GISci and some other conclusions.

2 Basic Morphologic Transformations

2.1 Basic Binary Morphologic Transformations

Dilation and erosion are basic mathematical morphologic operators [16], [20], [21]. These operations can be performed by employing the Boolean AND the Boolean OR operations [21] on any object, represented by the set X and its background by the set complement X^c (e.g., a map in binary form), of the two-dimensional euclidean discrete space Z^2 by means of a (window) set B. This B is called a *structuring element* that has a simple geometrical shape (e.g., disk) and a size (e.g., size of 3×3) smaller than the image X. We explain these transformations including their multiscale versions by following the notations followed in [20], [21].

The Boolean OR transformation of X by B is equivalent to the Minkowski set addition $\oplus$ of X by B. This operation that expands image object is also called dilation of X by B:

$$X \oplus B \triangleq \{z : (B^s)_{+z} \cap X \neq \emptyset\} = \bigcup_{y \in B} X_{+y}, \tag{1}$$

• *The author is with the Systems Science and Informatics Unit, Indian Statistical Institute-Bangalore Centre, 8th Mile, Mysore Road, RVCE PO, Bangalore 560059, India. E-mail: bsdsagar@isibang.ac.in.*

Manuscript received 18 Aug. 2008; revised 18 Feb. 2009; accepted 15 July 2009; published online 19 Aug. 2009.
Recommended for acceptance by P. Maragos.
For information on obtaining reprints of this article, please send e-mail to: tpami@computer.org, and reference IEEECS Log Number TPAMI-2008-08-0500.
Digital Object Identifier no. 10.1109/TPAMI/2009.163.

where X_{+y} denotes the *translation* of X along the vector y, $X_{+y} \triangleq \{x+y | x \in X\}$, and $B^s \triangleq \{x : -x \in B\}$ is the *symmetric* of B with respect to origin.

The Boolean AND transformation of X by B^s is equivalent to the Minkowski set subtraction $\ominus$ of X by B. This operation that shrinks the input image object is also called erosion of X by B:

$$X \ominus B \triangleq \{z : B_{+z} \subseteq X\} = \bigcap_{y \in B} X_{-y}. \quad (2)$$

Henceforth, we denote the dilation and erosion of X by B as $(X \oplus B)$ and $(X \ominus B)$. These transformations ((1) and (2)) can be performed by increasing the size of the structuring element to λB [20], where $\lambda = 0, 1, 2, \ldots, N$. The reader may want to refer to [16], [20], [21] for detailed explanations and implementations of these fundamental morphologic transformations along with their algebraic properties.

2.2 Hausdorff Erosion Distance and Hausdorff Dilation Distance

Let (X^t) and (X^{t+1}) be the nonempty compact sets at two time instants t and $t+1$. According to [13], the Hausdorff erosion distance $\sigma(X^t, X^{t+1})$ and the dilation distance $\rho(X^t, X^{t+1})$ between X^t and X^{t+1} are defined, respectively, as

$$\sigma(X^t, X^{t+1}) = \inf\{\lambda : [(X^t \ominus \lambda B) \subseteq X^{t+1}], [(X^{t+1} \ominus \lambda B) \subseteq X^t]\}, \quad (3)$$

$$\rho(X^t, X^{t+1}) = \inf\{\lambda : [X^t \subseteq (X^{t+1} \oplus \lambda B)], [X^{t+1} \subseteq (X^t \oplus \lambda B)]\}. \quad (4)$$

The Hausdorff dilation distance (introduced in [13]) is similar to the classic concept of "Hausdorff distance" [22]. Algebraically, these two distances yield metrics which are dual to each other with respect to the "complement" operation.

2.3 Computation of the Median Set

The median set [13], which is central to the theme of the paper, can be computed by employing multiscale erosions and dilations along with certain logical operations. If there exists a bijection between the sets (X^t) and (X^{t+1})—such that (X^t) is completely contained in (X^{t+1}), $(X^t \subseteq X^{t+1})$—the equation for computing the median set $M(X^t, X^{t+1})$ between (X^t) and (X^{t+1}) takes the form:

$$M(X^t, X^{t+1}) = \bigcup_{\lambda \geq 0} ((X^t \oplus \lambda B) \cap (X^{t+1} \ominus \lambda B)). \quad (5)$$

If (X^t) is only partially contained in (X^{t+1}), (5) takes the form:

$$M(X^t, X^{t+1}) = \bigcup_{\lambda \geq 0} ([(X^t \cap X^{t+1}) \oplus \lambda B] \cap [(X^t \cup X^{t+1}) \ominus \lambda B]), \quad (6)$$

where $M(X^t, X^{t+1})$ satisfies a more symmetrical property (see [13], [23]):

$$\begin{aligned} \mu &= \inf\{\lambda : \lambda \geq 0, (X^t \oplus \lambda B) \supseteq (X^{t+1} \ominus \lambda B)\} \\ &= \rho(X^t, M) = \sigma(M, X^{t+1}). \end{aligned} \quad (7)$$

$M(X^t, X^{t+1})$ is at Hausdorff dilation distance μ from (X^t), while $M(X^t, X^{t+1})$ is at Hausdorff erosion distance μ from (X^{t+1}). This further implies, for the case of $(X^t \subseteq X^{t+1})$, that $X^t \subseteq M \subseteq X^{t+1}$, and one has strictly $\rho(X^t, M) = \inf_{\lambda \geq 0}\{\lambda : M \subseteq (X^t \oplus \lambda B)\}$ and $\sigma(M, X^{t+1}) = \inf_{\lambda \geq 0}\{\lambda : (X^{t+1} \ominus \lambda B) \subseteq M\}$.

In what follows, (3)-(7), originally meant for global transforms that ignore connectivity, will be extended to companion-connected components X_i^t and X_i^{t+1} with index i of sets (X^t) and (X^{t+1})—with varied possible spatial relationships, between the time-dependent themes X^t and X^{t+1}(sets), given as categories. We assume that there exists a bijection between the connected components X_i^t of set (X^t) and the connected components X_i^{t+1} of set (X^{t+1}), for the various indices i. The categorization process based on spatial relationships between the companion-connected components of X^t and X^{t+1} would be clear after Section 3.1.

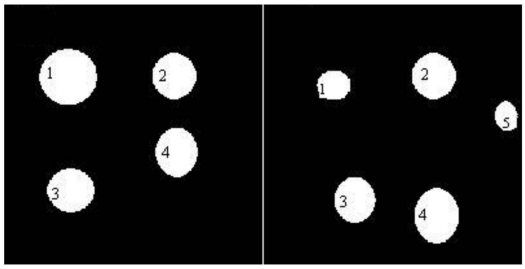

(a) (b)

Fig. 1. Two sets depicted in (a) and (b), respectively, represent corresponding subsets at two different time instants. These two sets are the inputs to generate a sequence of interpolated sets. The four categories explained in the text reflect in the four and five subsets, respectively, from the two input sets (a) and (b). Corresponding subsets of each panel are indexed with numerals. It should be noted that blobs with the same index from the two panels (a) and (b) belong to two different periods. If these two panels are superimposed, blobs with indexes 1 and 2 of panel (b) will be contained in blobs 1 and 2 of panel (a), further indicating that the spatial relationships fall under Category 1. Spatial relationships between the blobs with indexes 3 and 4 from the panels (a) and (b), respectively, fall under the categories 2 and 3, whereas blob 5, in the second panel, that does not possess a companion subset in the first panel falls under Category 4.

3 Layered Information as Sets: Spatial Interpolation

A procedure for generating continuous layers starting out from a limited set of layers is proposed in this section. Limited sets here refer to two input sets. The sequential steps involved to achieve the objective include:

1. extraction and description of layered information available at two different time periods;
2. establishing spatial relationships between the sets and also between the corresponding subsets of the two main subsets as well as categorization of the subsets based on the spatial relationships;
3. computation of the median set between two input sets;
4. generation of a sequence of interpolated sets based on the two input sets and the median sets thus generated.

3.1 Limited Layered Sets

The layered information depicting a specific phenomenon available for static systems or for a time-dependent (dynamic) system can be of three types: ordered, semiordered, or disordered. Let $X_1^t, X_2^t, \ldots, X_n^t$ and $X_1^{t+1}, X_2^{t+1}, \ldots, X_n^{t+1}$ be the connected components (e.g., lakes) at time periods "t" and "$t+1$" represented on Z^2 (Figs. 1a and 1b). For notational simplicity, we denote (X^t) and (X^{t+1}) as sets (layers) and represent the connected components—$X_1^t, X_2^t, \ldots, X_n^t$ and $X_1^{t+1}, X_2^{t+1}, \ldots, X_n^{t+1}$ as their subsets. X_i^t and X_i^{t+1}, $\forall i \in I$, are assumed always to be nonempty and compact. In what follows, "sets" and "layered data," as well as "subsets" and "connected components," are use interchangeablyd.

3.2 Spatial Relationships between Sets and Their Categorization

If $X^t \subseteq X^{t+1}$ or $X^{t+1} \subseteq X^t$, we say that these sets are *ordered sets*. The subsets embedded within each set at a respective time instant follow the relationship: $X_i^t \bigcap X_j^t = \emptyset$; $\forall t; i, j = 1, 2, \ldots, N; i \neq j$. We refer to (X^t) and (X^{t+1}) as a semi-ordered form if subsets of $X^t (resp. X^{t+1})$ are only partially contained in the other set X^{t+1} (respectively, X^t), whereas (X^t) and (X^{t+1}) are considered as

disordered sets if there arises an empty set while taking the intersection of (X^t) and (X^{t+1}) (or) of their corresponding subsets.

3.2.1 Description of Categories via Logical Relations

The evolution of subsets of X^t over a period of time depends upon some controlling factors, for example, temperature is one such factor of lake evolution. The corresponding subsets X^{t+1} explain the effect of controlling factor that causes changes in the subsets of X^t. By assuming that these subsets are lakes at time t and $t+1$, respectively, embedded in sets X^t and X^{t+1}, one can study the spatial behavior of these subsets by investigating the spatial relationship between each subset of X^t and its companion subset of X^{t+1}. Let us assume that there exists a bijection between the connected components X_i^t and X_i^{t+1} of sets X^t and X^{t+1}, respectively. Different possibilities, based on the relationships between the corresponding subsets of two layered data, are broadly classified in three groups as follows:

1. The categories that satisfy the condition $X_i^t \cap X_i^{t+1} \neq \emptyset$ for all $i \in I$, respectively, include: a) Category 1 if $X_i^t \subseteq X_i^{t+1}$ or $X_i^t \supseteq X_i^{t+1}$; $X_i^t = X_i^{t+1}$, $(X_i^t \cap X_i^{t+1}) = (X_i^t \cup X_i^{t+1}) \neq \emptyset$ and b) Category 2 if $X_i^t \not\subset X_i^{t+1}$ and/or $X_i^{t+1} \not\subset X_i^t$; $X_i^t \cap X_i^{t+1} \neq \emptyset$.
2. The sets X^t and X^{t+1} have the same number of connected components, but the conditions mentioned in categories 1 and 2 (group I) are not always satisfied in a situation (Category 3) where $X_i^t \cap X_i^{t+1} = \emptyset$.
3. Assume that X^t has less connected components than X^{t+1} (Category 4), but each X_i^t has a companion X_i^{t+1} such that one of the conditions given in the two categories of group I is satisfied. In some situations, for example, at the drought season t, a lake may become empty. Then, one can complete X^t by adding to it the ultimate erosions of those connected components of X_i^{t+1} that have no companion sets in X^t.

The four categories under the three groups have been conceived based on set theoretical and logical relations. The first two categories fall under group I due to the fact that the intersections between the connected components of X^t and X^{t+1} yield nonempty sets. Category 3 falls under group II as the intersection between the nonempty compact connected components yields an empty set, whereas Category 4 of group III has been conceived under the assumption that the intersection between the connected component(s), one of which is an empty set, yields the empty set. Clear distinction between Categories 3 and 4 of groups II and III can be seen in terms of variations in the properties of connected components of the companion sets.

For the sake of categorizing the corresponding connected components of layered data, whether or not they are connected components, there exist some methods in GISci literature strictly based on logical reasoning [1], [2], [3], [4], [5].

3.2.2 Description of Categories Using Hausdorff Distances

Connected components with companions between two sets that belong to two different time instants can be categorized quantitatively with respect to their spatial relations and Hausdorff distances.

Category 1. The connected components for which both $\rho(X_i^t, X_i^{t+1})$ and $\sigma(X_i^t, X_i^{t+1})$ are zero are considered to be Category 1 of group I and they follow one of the following three conditions: 1) $X_i^t \subseteq X_i^{t+1}, \forall i \in I$; 2) $X_i^t \supseteq X_i^{t+1}$; and 3) $(X_i^t \cap X_i^{t+1}) = (X_i^t \cup X_i^{t+1}) \neq \emptyset$. According to [13] and (3) and (4), $\sigma(X_i^t, X_i^{t+1}) = \rho(X_i^t, X_i^{t+1}) = 0$ for these three conditions. By (3), we can explain why $\sigma(X_i^t, X_i^{t+1})$ yields zero for condition 1) in three steps a)-c): a) The zeroth-eroded version of X_i^t (i.e., $(X_i^t \ominus 0B)$) would become a subset of X_i^{t+1}; b) X_i^{t+1} would become a subset of X_i^t only after a finite number of erosions; and c) the minimum of λ obtained from steps a) and b), involved in the erosion process, is zero. According to (4), for condition 1), the following three steps p)-r) explain why $\rho(X_i^t, X_i^{t+1})$ yields zero: p) X_i^t would become a subset of zeroth-dilated version of X_i^{t+1} (i.e., $(X_i^{t+1} \oplus 0B)$); q) X_i^{t+1} would become a subset of some finite dilated version of X_i^t; and r) the minimum of λ obtained from steps p) and q), involved in the dilation process, is zero. These three-step explanations are also true with conditions 2) and 3).

TABLE 1
Categorywise Hausdorff Distances

Group	Category	$\sigma\left(X_i^t, X_i^{t+1}\right)$	$\rho\left(X_i^t, X_i^{t+1}\right)$
I	1	0	0
I	2	≥ 1	≥ 1
II	3	Does not exist	≥ 1
III	4	Does not exist	Does not exist

Category 2. If both $\sigma(X_i^t, X_i^{t+1})$ and $\rho(X_i^t, X_i^{t+1})$ are finite distances (i.e., ≥ 1), then the involved connected components X_i^t and X_i^{t+1} are considered to be of Category 2 of group I. Such categorized connected components strictly follow the conditions: 1) $X_i^t \cap X_i^{t+1} \neq \emptyset$ and 2) $X_i^t \not\subset X_i^{t+1}$.

Category 3. If only $\rho(X_i^t, X_i^{t+1})$ yields a finite distance (i.e., ≥ 1) between X_i^t and X_i^{t+1}, and there is no possibility to compute $\sigma(X_i^t, X_i^{t+1})$—as no degree of erosion of either of the involved (corresponding) subsets make the eroded set being contained in the other corresponding subset—then the spatial relationship between X_i^t and X_i^{t+1} is considered to be of Category 3 of group II. Such category appears only when $X_i^t \cap X_i^{t+1} = \emptyset$.

Category 4. Those nonempty connected components of X^{t+1} that have no companion subsets in X^t and for which neither of the Hausdorff distances exist are categorized as Category 4 of group III. To compute recursive median elements under such unique situation, one can complete X^t by adding to it the ultimate erosions $(UX_i^{t+1} \neq \emptyset)$ of those connected components of X_i^{t+1} that have no companion sets in X^t. The ultimate erosion of X_i^{t+1}, (UX_i^{t+1}), retains the final pixel value just before the last erosion that changed X_i^{t+1} to 0. Note that both $\sigma(X_i^{t+1}, UX_i^{t+1})$ and $\rho(X_i^{t+1}, UX_i^{t+1})$ yield zero distance according to (3) and (4).

The relationships categorized above are dependent on the controlling factor. For instance, if the changes in the areal extent of lakes over a period of time have occurred due to a change in the temperature regimes, then the geometric evolution of lakes with evolving temperature fields can be computed by constructing interpolated layered maps. Table 1 depicts the possible Hausdorff distances both by erosion and dilation for the different categories.

The categorization of connected components based on spatial relations between the connected components (X_i^t) and their companions (X_i^{t+1}) of X^t and X^{t+1} can be done directly by computing $\sigma(X_i^t, X_i^{t+1})$ and $\rho(X_i^t, X_i^{t+1})$ without checking for logical relationships (conditions). Checking the duality property of metrics $\sigma(X_i^t, X_i^{t+1})$ and $\rho(X_i^t, X_i^{t+1})$, the intersections of the sets—between which these distances need to be computed—must be within the four categories mentioned above. This validation further provides a basis: 1) to properly categorize the sets and/or their corresponding subsets and 2) to test the quality of interpolations. In order to generate a sequence of interpolations between the categorywise connected components, (5) and (6) form the basis to compute median elements between X_i^t and X_i^{t+1} of sets X^t and X^{t+1}.

3.3 Morphologic Interpolation via Median Element Computation

The median set $M(X^t, X^{t+1})$ between two sets X^t and X^{t+1}, according to (5) and (6), is a global transform that ignores connectivity. But, in some situations, it is required to introduce a

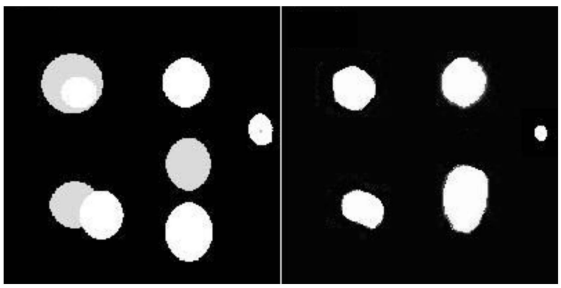

(a) (b)

Fig. 2. (a) Two layers (sets) consisting of subsets with various spatial relationships shown in the two panels of Fig. 1 are superimposed. (b) Computed median sets between the corresponding input subsets as shown in Figs. 1a and 1b.

bijection between the connected components X_i^t and X_i^{t+1} of X^t and X^{t+1}, respectively. In order to better visualize these spatially evolving subsets, one has to generate interpolated sequences of subsets at successive time instants in layered forms. The computation of the interpolated (median) layer $M(X_i^t, X_i^{t+1})$ between the layers X^t and X^{t+1} is category-dependent. To get an intermediary set between X^t and X^{t+1}, i.e., $X^{\frac{t+1}{2}}$, we use (5) and (6). Categorywise geometric interpretations and median element computations between the companion-connected components are illustrated in Figs. 2a and 2b and summarized in (8)-(13).

Category 1 with $X_i^t \subseteq X_i^{t+1}$:

$$M\big(X_i^t, X_i^{t+1}\big) = \bigcup_{\lambda=0}^{N} \big(X_i^t \oplus \lambda B\big) \cap \big(X_i^{t+1} \ominus \lambda B\big). \tag{8a}$$

Category 1 with $X_i^t \supseteq X_i^{t+1}$:

$$M\big(X_i^{t+1}, X_i^t\big) = \bigcup_{\lambda=0}^{N} \big(X_i^t \ominus \lambda B\big) \cap \big(X_i^{t+1} \oplus \lambda B\big). \tag{8b}$$

Category 1 with $(X_i^t \cap X_i^{t+1}) = (X_i^t \cup X_i^{t+1}) \neq \emptyset$:

$$M\big(X_i^t, X_i^{t+1}\big) = X_i^t = X_i^{t+1}. \tag{9}$$

Category 2 with either $X_i^t \not\subset X_i^{t+1}$ or $X_i^{t+1} \not\subset X_i^t$:

$$M\big(X_i^t, X_i^{t+1}\big) = \bigcup_{\lambda=0}^{N} \big(\big(X_i^t \cup X_i^{t+1}\big) \ominus \lambda B\big) \cap \big(\big(X_i^t \cap X_i^{t+1}\big) \oplus \lambda B\big). \tag{10}$$

If X_i^t and X_i^{t+1} are at least partially connected, such that $X_i^t \cap X_i^{t+1} \neq \emptyset$ (e.g., Categories 1 and 2), then all possible median elements that could be generated through morphologic interpolation between the subsets X_i^t and X_i^{t+1}, and also between recursively generated median sets, are at least partially overlapping. A variant of (10) was proposed and discussed in [23]. Since there is a bijection between the connected components X_i^t and X_i^{t+1} of $(X^t), (X^{t+1})$, that fall under Categories 1 and 2 of Group I, one can prove that

$$M\big(X^t, X^{t+1}\big) = \bigcup_{\forall i} M\big(X_i^t, X_i^{t+1}\big). \tag{11}$$

Category 3: Equation (11) does not hold for this category. One can modify the data by using the construction that results in (12). Let X_i^t, X_i^{t+1}, $CH(X_i^t \cup X_i^{t+1})$, respectively, be the subsets of (X^t), (X^{t+1}) and the convex hull of the union of subsets X_i^t and X_i^{t+1}. Let these subsets and/or sets be nonempty compact, and $(X_i^t, X_i^{t+1}) \subseteq CH(X_i^t \cup X_i^{t+1})$. $M_1(X_i^t, CH(X_i^t \cup X_i^{t+1}))$ and $M_2(X_i^{t+1}, CH(X_i^t \cup X_i^{t+1}))$ are median sets, respectively, between X_i^t and $CH(X_i^t \cup X_i^{t+1})$ and X_i^{t+1} and $CH(X_i^t \cup X_i^{t+1})$. Such median sets M_1 and M_2 as well as the median set $M_s = M(M_1, M_2)$ satisfy the following conditions: 1) $M_1 \neq \emptyset$; $M_2 \neq \emptyset$; 2) $M_1 \cap M_2 \neq \emptyset$; and 3) $M(M_1, M_2) \neq \emptyset$, so that:

$$M_s = M(M_1, M_2) = \bigcup_{\lambda=0}^{N} [(M_1 \cap M_2) \oplus \lambda B] \cap [(M_1 \cup M_2) \ominus \lambda B]. \tag{12}$$

Category 4: Median elements which under unique situation arise in Category 4 of group III can be computed as:

$$M\big(X_i^t, X_i^{t+1}\big) = \bigcup_{\lambda=0}^{N} \big(UX_i^{t+1} \oplus \lambda B\big) \cap \big(X_i^{t+1} \ominus \lambda B\big), \tag{13}$$

where UX_i^{t+1} is the ultimate eroded version of X_i^{t+1}.

3.4 Sequence of Interpolated Sets

Using the median set, the interpolation sequence can be obtained recursively. Let X_i^t and X_i^{t+k} denote the input subsets, k denotes time gap between two successive maps, and n the recursion level (always a power of 2) and let $X_i^{t+(\frac{k}{2^n})}$ or $M(X_i^t, X_i^{t+k})$ denote the median element between two input subsets. The median element between two input companion-connected components X_i^t and X_i^{t+k}, respectively, belonging to the two time instants t and $t+k$, is also denoted by $X_i^{t+(\frac{k}{2^1})} = X_i^{t+(\frac{k}{2})}$. Then, the sequence of interpolated sets, between two inputs X_i^t and X_i^{t+k}, is defined as

$$X_i^{t+\left(\frac{k}{2^1}\right)} = M\big(X_i^t, X_i^{t+k}\big); X_i^{t+\left(\frac{k}{2^2}\right)} = M\left(X_i^t, X_i^{t+\left(\frac{k}{2^1}\right)}\right); \ldots. \tag{14}$$

In $X_i^{t+(\frac{k}{2})}$, the superscript $t+(\frac{k}{2})$ denotes the intermediary time. For instance, the two successive maps X^t and X^{t+k} available are for years $t = 1896$ and $t+k = 1898$, where the time gap (k) is 2. Then, the superscript for the median element, generated by taking these two input maps, should be 1897. The median element at intermediary time is $X_i^{1896+(\frac{2}{2^1})} = X_i^{(1897)}$.

The maximum possible number of layers $(N_{\max})$ that can be generated (interpolated) between the input layers (sets) X^t and X^{t+1} including two input layers is given by

$$\begin{aligned}(N_{\max}) = \max\{&[\min(\lambda : X^{t+1} \subseteq (X^t \oplus \lambda B))],\\ &[\min(\lambda : X^t \subseteq (X^{t+1} \ominus \lambda B))]\}.\end{aligned} \tag{15}$$

4 Experimental Results

The ideas in the previous section have been employed in practical examples to demonstrate their applicability. To demonstrate the applications of the Hausdorff distance for understanding the spatial relations between two discrete maps in general and between the companion-connected components in particular and to generate maximum possible sequential maps, we consider spatially represented 1) small water bodies, retrieved from remotely sensed data of peak drought (X^t) and peak monsoon (X^{t+1}) periods as basic inputs and 2) bubonic plague epidemic data available at annual intervals during the period 1896-1906.

4.1 Case Study on Small Water Bodies

We chose two input synthetic sets, depicting small water bodies represented by 512×512 binary pixels, at peak drought period (Fig. 3a) and peak flood period (Fig. 3b), respectively. These two input slices fall under Category 1 (see Section 3.2), so we employ (8a) to generate an interpolated slice (median set) (Fig. 3c).

By using the median set thus generated, a sequence of interpolated slices is recursively generated, as shown in Fig. 4.

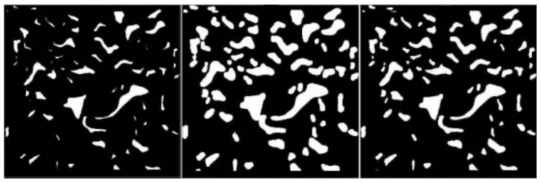

Fig. 3. (a) Input slice 1, lakes (in peak drought time) in binary format. (b) Lakes (in peak flood time) as input slice 2. (c) Median set computed between two input slices shown in (a) and (b).

Including two input slices, a total of five slices are generated as $(N_{\max})$ computed for the two input slices is 5 according to (15).

4.2 Case Study on Spatial Maps of Epidemic

Spatial maps depicting bubonic plague data—available for a period of 11 years during 1896-1906 at annual intervals, generated by Yu and Christakos [24]—were chosen. We applied the methodology explained in the previous case study by choosing the spatial maps of successive years (Figs. 5a, 5b, 5c, 5d, 5e, 5f, 5g, 5h, 5i, 5j, and 5k) to generate a sequence of interpolated maps between the sets of maps of successive years to visualize the spread of epidemics in a continuous manner.

According to the spatial relation between the successive spatial maps, which are ordered and/or semi-ordered sets, both $\rho(X^t, X^{t+1})$ and $\sigma(X^t, X^{t+1})$ yield ≥ 1. Hence, they are classified as Category 2. According to (7), the μ for the first-level median sets for both successive maps (i.e., X^t and X^{t+1}), and also for X^t and X^{t+2} is computed for all t values (Table 2). This μ provides an estimate of the maximum number of interpolated maps that could be generated.

4.2.1 Validation of the Middle Elements as Interpolators

For this epidemic case, involving 11 yearly maps for the geographic spread of bubonic plague in India, while testing for the quality of the middle element as an interpolator (Fig. 6) we made comparisons between $M(X^t, X^{t+2})$ with X^{t+1}, for all possible t.

This data further provide the distribution of the rate of spread in terms of μ computed for the data of successive years (Table 2). The higher the μ, the more rapid is the rate of spread. For instance, between the years 1897 and 1898, 1898 and 1899, 1900 and 1901, 1901 and 1902, as well as between 1902 and 1903, the rates of spread of plague were significantly faster than in the other periods. By considering the spatial maps of years 1896 and 1897, a maximum of six spatial maps could be generated by using (8)-(14). The interpolated maps computed from 10 pairs of maps at annual intervals during the period 1896-1906 can be employed to generate an animation depicting the way the epidemic spread spatially in a continuous manner (See animation as.avi file at http://www.isibang.ac.in/~bsdsagar/Epid-animate2.avi). This

Fig. 4. A sequence of interpolated sets (slices) in between two input slices, as shown in Figs. 3a and 3b. Equations (8a) and (14) are used to recursively generate the interpolated slices. The layer depicting water bodies with magenta color is the median set, as shown in Fig. 3c.

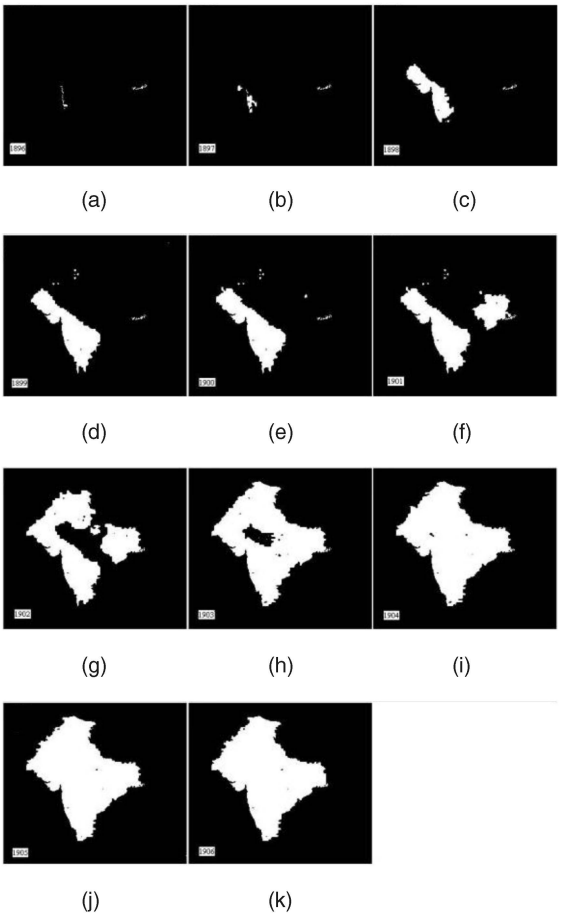

Fig. 5. (a)-(k) Spatial temporal maps that represent the geographic spread of bubonic plague in India between 1896 and 1906 at intervals of one year [24]. The 11 spatial maps depicting the spread of plague were sequentially used to generate the maximum possible number of interpolated maps.

procedure paves the way to generate continuous slices between two input slices recorded at significantly different instants of time.

We found a significantly reasonable quality for the median sets $M(X^t, X^{t+2})$ generated for the epidemic data between alternative years as interpolators. The median sets were tested by comparing $M(X^t, X^{t+2})$ with X^{t+1} for all possible t. There obviously exists a significant match between the interpolated median elements (Figs. 6b, 6c, 6d, 6e, 6f, 6g, 6h, 6i, and 6j)—computed between the real data X^t and X^{t+2} that belong to nine pairs of maps (Table 2)—and the real data (Figs. 5b, 5c, 5d, 5e, 5f, 5g, 5h, 5i,

TABLE 2
μ Values Computed for X^t and X^{t+1} and X^t and X^{t+2}

t, t+1, t+2	μ	
	$M(X^t, X^{t+1})$	$M(X^t, X^{t+2})$
1896, 1897, 1898	3	9
1897, 1898, 1899	9	15
1898, 1899, 1900	11	11
1899, 1900, 1901	2	12
1900, 1901, 1902	12	15
1901, 1902, 1903	13	16
1902, 1903, 1904	9	14
1903, 1904, 1905	7	7
1904, 1905, 1906	2	2
1905, 1906, -	1	-

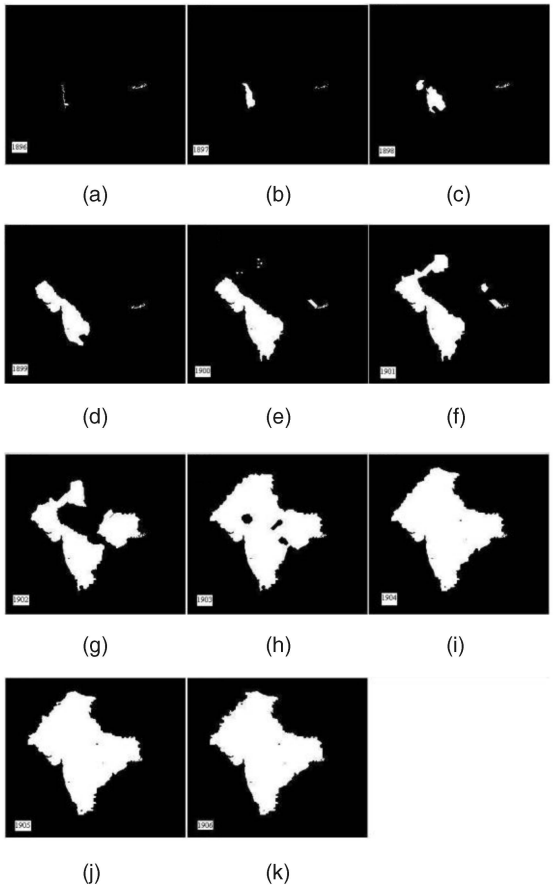

Fig. 6. (a) Original spatial map of the bubonic plague during 1896. (b)-(j) The first-level median sets computed for $M(X^t, X^{t+2})$ for all "t," ranging from 1896 to 1905. (k) Original spatial map during 1906. For validation, the maps of Figs. 6b, 6c, 6d, 6e, 6f, 6g, 6h, 6i, and 6j obtained as first-level median sets $M(X^t, X^{t+2})$ are, respectively, compared for all "t" with those t of Figs. 5b, 5c, 5d, 5e, 5f, 5g, 5h, 5i, and 5j. These first-level median sets show a reasonable matching with the actual sets (Figs. 5b, 5c, 5d, 5e, 5f, 5g, 5h, 5i, and 5j).

and 5j). For the sake of a better visual comparison, we also represent the original spatial maps (Figs. 5a, 5b, 5c, 5d, 5e, 5f, 5g, 5h, 5i, 5j, and 5k) and the spatial maps generated according to $M(X^t, X^{t+2})$ (Figs. 6a, 6b, 6c, 6d, 6e, 6f, 6g, 6h, 6i, 6j, and 6k) in a composite way by superimposing them on one another and assigning gray shade to each original spatial map as well as maps generated via median set computation (Figs. 7a and 7b).

The Hausdorff dilation and erosion distances were computed between $M(X^t, X^{t+2})$ and X^{t+1} for all t values (Table 3) to test the quality of interpolation. These distances were compared with the respective Hausdorff dilation and erosion distances of X^t and X^{t+1}

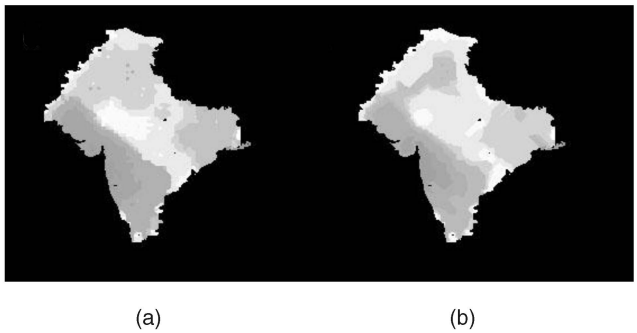

Fig. 7. Superimposed gray-coded (a) original spatial maps and (b) spatial maps generated *via* median set computations.

TABLE 3
Hausdorff Distance Values

t	$\rho[M(X^t, X^{t+1}), X^{t+1}]$	$\sigma[M(X^t, X^{t+1}), X^{t+1}]$	$\rho(X^t, X^{t+1})$	$\sigma(X^t, X^{t+1})$
1896	8	2	7	1
1897	2	2	1	1
1898	1	1	1	1
1899	4	2	1	1
1900	12	9	1	1
1901	8	7	2	1
1902	8	8	1	1
1903	3	3	2	1
1904	2	2	1	1
1905	-	-	2	1

(Table 3). The lower the difference between the values of $\rho[M(X^t, X^{t+1}), X^{t+1}]$ or $\sigma[M(X^t, X^{t+1}), X^{t+1}]$ and $\rho(X^t, X^{t+1})$ or $\sigma(X^t, X^{t+1})$ is, the higher the degree of matching is. Mismatch between the interpolated and actual maps is observed in terms of these values for the interpolated maps for the t values of 1896 and 1901. This slight discrepancy in the values for the years 1896 and 1901 is due to the presence of a few spikes related to the connected component(s) of one of the two input sets. Other maps in the sequence have exhibited a significantly higher degree of matching. For all cases shown in the last four columns of Table 3, the Hausdorff erosion distances are found to be slightly less than the Hausdorff dilation distances. However, the fair overall matching further signifies that the interpolations are valid.

From this comparison of the real and interpolated maps, we conclude that: 1) There exists a significant match between the real data and the data generated as median sets and 2) by comparing $M(X^t, X^{t+2})$, one cannot expect to exactly obtain X^{t+1} due to the fact that μ computed for X^t and X^{t+2} may not be exactly the same as $\rho(X^t, X^{t+1})$. The success of this interpolation relies on the time gap (k) between the successive maps considered to generate median maps. The smaller the (k) is, the higher the approximation is, and, in turn, the interpolated maps geometrically conform well to the realistic maps as shown in the results. Better approximations could be expected when the time interval between two input maps is smaller. On the contrary, the degree of geometric similarity between the maps generated via median map computation and the realistic maps may be poor as in the case of many other interpolation techniques. For instance, the median map, obtained by taking the 1896 and 1904 maps (Figs. 5a and 5i) as two input maps, may not show significant match with the realistic map of year 1900 (Fig. 5e). This is due to the fact that the time gap (k) between two input maps is eight years.

5 Potential Applications: A Brief Discussion

Prediction is a challenging task to model/simulate/visualize the general spatiotemporal behavior of any kind of phenomena, including, to name a few, spreads of rainfall, flood water, lakes, epidemics, population, cities, elevation structures, temperatures, hurricanes, soil moisture, earth resistivity, clouds, impact of sea level rise on the landmass, etc. The reader will certainly find several different examples where one can apply the framework shown here. Two specific examples where one can apply the discussed interpolation technique for discrete spatial and/or temporal themes are the following:

1. Generation of contours from sparse DEM data: One can generate intermediary contours to create spatially distributed elevation regions with dense elevation contours from

sparse elevation contours. For this case, successive elevation regions, which are usually in ordered form, need to be decomposed via threshold decomposition [25]. Due to the coarse spatial resolution of the data, the spatial gap between any two successive threshold decomposed elevation regions is significantly larger than that of the finer resolutions. To generate intermediary elevation regions between such coarser successive elevation regions, one can follow the median set computation approach that is meant for Category 1. Kriging is appropriate technique to deal with the maps of this Category 1. In most of its applications, simple euclidean distance has been employed to define the separation between the sample points. It has been known that euclidean distance is not always an appropriate metric to define the separation between the points. But, this framework employs non-euclidean metrics, such as Hausdorff erosion and Hausdorff dilation distances, to develop median set(s).

2. Spatiotemporal behavior of lakes: The geometries of a group of lakes at (at least) two different time instants are mapped as layered information and stored in GIS database. One can employ the aforementioned framework to analyze how the groups of lakes have geometrically evolved between the successive time periods. For this case, maps depicting lakes, retrieved from remotely sensed data at two significantly staggered time periods (e.g., peak monsoon time and peak drought time within a year), can be considered to generate several possible intermediary layers of lakes. Such a study would provide insight to the spatiotemporal organization of the lakes.

6 Conclusions

The recursive generation of interpolated layers (sets), in between two input slices and/or median sets thus generated, is a challenge in the context of Geographic Information Sciences. Morphologic interpolation via median set computation is one of the ways to deal with spatial interpolation. We propose a framework to describe the spatial relations between the corresponding subsets of two input sets. Four possible spatial relationships between the corresponding subsets are categorized. This categorization is done based on both by logical relationships and Hausdorff distances. Mathematical morphologic transformations are employed to: 1) measure the Hausdorff erosion and dilation distances between the corresponding subsets in particular, and between the input sets in general and 2) compute a sequence of interpolated slices. Results have been demonstrated on synthetic sets, small water bodies in two different seasons, and also on spatial maps depicting the spread bubonic plague through 11 years. Further, the quality of median elements as interpolators were evaluated. This framework that complements already existing interpolation methods provides potentially valuable insights in the context of GISci. Supplemental materials for this paper are available in the Computer Society Digital Library at http://doi.ieeecomputersociety.org/10.1109/TPAMI.2009.163.

Acknowledgments

The author is most grateful to the three anonymous reviewers, and to Professor Jean Serra and Professor Petros Maragos for their highly useful comments and suggestions on the manuscript, which have led to significant improvements both in content and quality. He also gratefully acknowledges the encouragement given by the associate editor, Professor Petros Maragos, who expertly handled the earlier versions of this paper. He is also grateful to Professor Gabor Korvin for his useful suggestions and comments on this manuscript.

References

[1] M. Worboys and M. Duckam, *GIS: A Computing Perspective.* CRC Press, 2004.
[2] A.U. Frank, "GIS for Politics," *Proc. Ann. Conf. GIS Planet '98* 1998.
[3] R.T. Snodgrass, "Temporal Databases," *Theories and Methods of Spatiotemporal Reasoning in Geographic Space,* A.U. Frank, I. Campari, and U. Formentini, eds., pp. 22-64, Springer-Verlag, 1992.
[4] C.D. Tomlin, *Geographic Information Systems and Cartographic Modeling.* Prentice Hall, 1990.
[5] S.M. Lane and G. Birkhoff, *Algebra.* Macmillan, 1967.
[6] A.U. Frank, "Map Algebra with Functors for Temporal Data," *Proc. ER Workshop Conceptual Modeling for Geographic Information Systems,* 2005.
[7] N.C. Cressie, *Statistics for Spatial Data.* John Wiley and Sons, 1993.
[8] G.T. Herman, J. Zheng, and C.A. Bucholtz, "Shape-Based Interpolation," *IEEE Computer Graphics and Applications,* vol. 12, no. 3, pp. 69-79, May 1992.
[9] S.P. Raya and J.K. Udupa, "Shape Based Interpolation of Multidimensional Objects," *IEEE Trans. Medical Imaging,* vol. 9, no. 1, pp. 32-42, Mar. 1990.
[10] S. Beucher, "Interpolation d'Ensembles, de Partitions et de Fonctions," Technical Report N-18/94/MM, Ecole des Mines de Paris, 1994.
[11] F. Meyer, "Interpolations," Technical Report N-16/94/MM, Ecole des Mines de Paris, 1994.
[12] J. Serra, "Interpolations et Distance de Hausdorff," Technical Report N-15/94/MM, Ecole des Mines de Paris, 1994.
[13] J. Serra, "Hausdorff Distances and Interpolations," *Math. Morphology and Its Applications to Images and Signal Processing,* H.J.A.M. Heijmans and J.B.T.M. Roerdink, eds., Kluwer Academic Publishers, 1998.
[14] M. Iwanowski, "Application of Mathematical Morphology to Image Interpolation," PhD thesis, School of Mines Paris—Warsaw Univ. of Technology, 2000.
[15] J. Vidal, J. Crespo, and V. Maojo, "Recursive Interpolation Technique for Binary Images Based on Morphological Median Sets," *Proc. Int'l Symp. Math. Morphology: 40 Years On,* C. Ronse, L. Najman, and E. Decenciere, eds., pp. 53-62, 2005.
[16] J. Serra, *Image Analysis and Mathematical Morphology.* Academic Press, 1982.
[17] D.J. Burr, "Elastic Matching of Line Drawings," *IEEE Trans. Pattern Analysis and Machine Intelligence,* vol. 3, no. 6, pp. 708-713, Nov. 1981.
[18] S.Y. Chen, W.C. Lin, C.C. Liang, and C.T. Chen, "Improvement on Dynamic Elastic Interpolation Technique for Reconstructing 3-D Objects from Serial Cross Sections," *IEEE Trans. Medical Imaging,* vol. 9, no. 1, pp. 71-83, Mar. 1990.
[19] P.N. Werahera, G.J. Miller, G.D. Taylor, T. Brubaker, F. Danesghari, and E.D. Crawford, "A 3-D Reconstruction Algorithm for Interpolation and Extrapolation of Planar Cross Sectional Data," *IEEE Trans. Medical Imaging,* vol. 14, no. 4, pp. 765-771, Dec. 1995.
[20] P. Maragos, "Pattern Spectrum and Multiscale Shape Representation," *IEEE Trans. Pattern Analysis and Machine Intelligence,* vol. 11, no. 7, pp. 701-716, July 1989.
[21] P. Maragos, "Morphological Filtering for Image Enhancement and Feature Detection," *The Image and Video Processing Handbook,* A.C. Bovik, ed., pp. 135-156, Elsevier Academic Press, 2005.
[22] F. Hausdorff, *Grundzuge der Mengenlchre.* Viet and Co. (Gekurzte) Auft., 1914.
[23] M. Iwanowski and J. Serra, "The Morphological-Affine Object Deformation," *Mathematical Morphology and Its Applications to Image and Signal Processing,* J. Goutsias, L. Vincent, D.S. Bloomberg, eds., pp. 81-90, Kluwer Academic Publishers, 2000.
[24] H.-L. Yu and G. Christakos, "Spatio-Temporal Modeling and Mapping of the Bubonic Plague Epidemics in India," *Int'l J. Health Geographics,* vol. 5, no. 12, 2006, doi: 10.1186/1476-072X-5-12.
[25] P. Maragos and R.D. Ziff, "Threshold Superposition in Morphological Image Analysis Systems," *IEEE Trans. Pattern Analysis and Machine Intelligence,* vol. 12, no. 5, pp. 498-504, May 1990.